A Highly Nonlinear Spiral Photonic Crystal Fiber for Tailoring Two Zero Dispersion Wavelengths in the Visible Region

Muhammad Nazmul Hossain[*], M. Shah Alam[#], Dihan Md. Nuruddin Hasan, and K. M. Mohsin

Electrical and Elecronic Engineering, Bangladesh University of Engineering and Technology (BUET)

Abstract—A dispersion flattened, spiral silica photonic crystal fiber (SSPCF) is presented here for supercontinuum generation in the visible region. Two zero dispersion wavelengths (ZDWs) (570nm & 630nm) are obtained in the visible region for a core diameter of 600nm and the range of the anomalous dispersion increasing with the increment of the core diameter. The fiber shows high nonlinearity parameter ($1433W^{-1}km^{-1}$), high Raman gain ($698.478W^{-1}km^{-1}$), ultraflattened dispersion (-0.05064 $ps/nm^2 \cdot km$) and very low confinement loss (0.00161 dB/km) at 600 nm. The proposed SSPCF shows improvement over the dispersion control of a hexagonal PCF, and low damage threshold of a highly nonlinear (HN) soft glass PCF. So it can be an excellent candidate for generating supercontinuum in the visible region with HeNe laser of pump wavelenght at 612nm.

A micro-structured photonic crystal fiber (MSPCF) inhibits easy manipulation of its dispersion curve and high nonlinear properties by tactful arrangement of air holes and core-cladding geometry. It has become the topic of extensive research for supercontinuum generation (SCG) since the work done by Ranka group in 2000 [1]. In SCG, tailoring the dispersion to achieve flat, anomalous dispersion with a small slope and zero crossing near/at the pump wavelength is an extremely important aspect [2]. Pumping near ZDW with higher nonlinearity not only reduces its power requirement but also smoothes the generated SC power spectra [3]. It has already been reported that silica PCF with asymmetrical air hole distribution provides maximum nonlinearity possible, whereas a very small improvement over the symmetric case may be obtained [4]. A soft glass equiangular spiral PCF has already been reported to be a suitable candidate for SCG in near infrared due to its higher nonlinearity ($\approx 5250W^{-1}km^{-1}$) [4]. However, SCG being pumped at the visible region should be an important phenomenon due to its embedded application in nanoscopy, confocal microscopy, and flow cytometry [6]. But, SCG in highly nonlinear soft glass, schott SF6, bismuth oxide, and tellurite PCFs using long pump pulses (ns) in the visible region is difficult, possibly because of the low damage threshold of these glasses. Silica is superior in the visible region due to its few orders of magnitude higher damage threshold than the above mentioned nonlinear materials [6].

E-mail: [#]shalam@eee.buet.ac.bd, [*]istigfar@gmail.com

Moreover, the nonlinearity of silica PCFs can be enhanced by doping germanium or fluorine as a dopant in the core region due to their enhanced nonlinear or Kerr refractive index. Therefore, in this work we engineered the spiral PCF design architecture [4] in silica material to achieve nearly zero ultraflattened dispersion curves with higher nonlinearity in the visible region. In this work, the design is proposed being inspired by the asymmetric seed distribution pattern of a sunflower and spiral compact architecture of a cauliflower. Additionally, four elliptical air holes surrounding the core introduced and increasing radii of air holes towards the outer edge of cladding is considered. The analysis of this work was carried out using a full-vector FEM [8], which allows the determination of optical mode field distributions of the pump and signal over the entire cross section of the fiber.

Figure 1 shows the cross sectional view of the spiral PCF designed in this work. The fiber material is silica and the core is germanium doped with a mole fraction of 40%. Four relatively larger elliptical air holes surround the core and act as inner cladding. The outer cladding air hole distribution is composed of 11 spiral arms each containing 6 air holes.
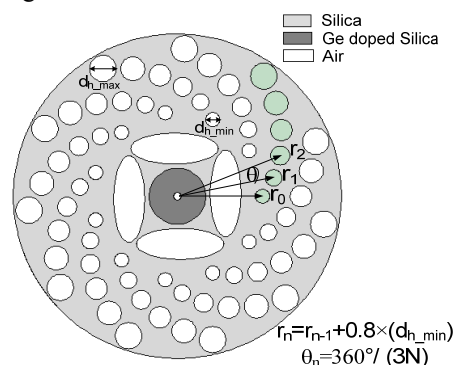

Fig. 1. Cross section of the spiral PCF.

In each spiral arm the first air hole is at a distance of r_0 from the center and each successive air holes are placed at an angular displacement of θ. The distance of the nth air hole of that spiral arm is $r_n = r_{n-1} + 0.8 \times (d_{h\_min})$ with an angular displacement of $\theta_n = 360^\circ/(3 \times N)$ from the previous hole of the spiral arm. Here, N is the total number of

spiral arm and d_{h_min} is the diameter of the first air hole in each arm. The diameters of air holes (d_h) in each spiral arm are smaller near the core and become larger gradually. Again, a small air hole of diameter d_c, is introduced in the core to make the core defective and to manipulate the dispersion curve. For the cross section shown in Fig. 1, r_0=0.9 µm, d_{h_max}=0.358 µm, and d_{h_min}=0.15 µm, and d_c=60 nm. The semi-axes of elliptical air holes ar: a=165 nm and b=462nm.
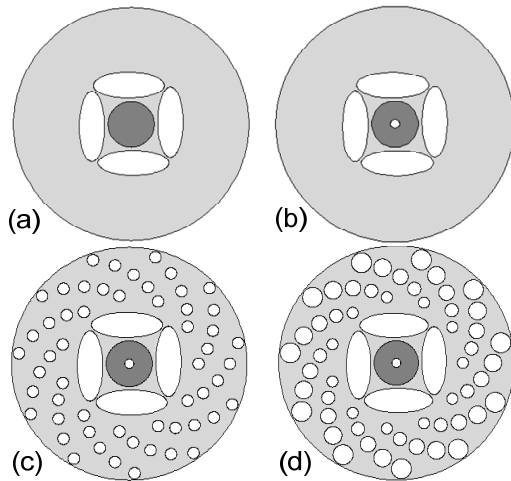

Fig. 2. Step by step design procedure a) array of elliptical air holes,   b) air hole defect in the core, c) spirally distributed cladding air holes without increment, and d) increment of cladding air holes for flattening dispersion.

Figure 2 shows the step by step design procedure for obtaining a highly nonlinear dispersion flattened PCF in the visible region. The complex structure is composed of

1. Inner cladding: rectangular array of four elliptical air holes for ultrahigh confinement irrespective of outer cladding (Fig. 2(a)) [9].
2. Inclusion of air hole at the center of the core: an air hole at the center of the core for shifting the dispersion curve up and down (Fig. 2(b)) [10].
3. Outer cladding: spirally distributed air holes for easy manipulation of dispersion curve (Fig. 2(c)) [4].
4. Gradual increment of air holes in each spiral arm for flattening the dispersion curve (Fig. 2(d))

The proposed fiber may be fabricated by using the sol-gel technique, which has already been used for fabricating PCF of various irregular structures [12]. As a casting method, the sol-gel technique can fabricate any structure, which can be assembled into a mold. The air hole size, shape and spacing may all be adjusted independently.

For obtaining the proposed silica preform consisting of air holes of different diameter, the initial outer cladding air holes (Fig. 2c) can be etched with HF (Hydrogen floried) for different period of time to get the desired design (Fig. 2d).

Nevertheless, input and output coupling in PCFs becomes more difficult as core size decreases. The transitions simplified input and output coupling may be used to efficiently excite the core of submicron diameter as shown in Fig. 3. For an endface diameter of 8.2 µm, it can be coupled to the laser source with a conventional SMF-28 fiber.
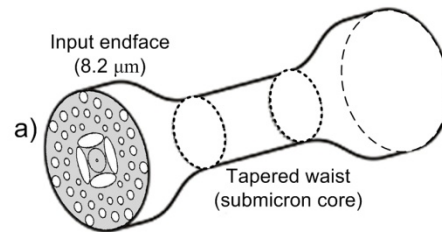

Fig. 3. Tapering a PCF to make a submicron core in the waist and facilitate input coupling.

However, by tapering "fast-and-cold", i.e., with relatively high elongation rate and low flame temperature for high drawing stress, the microstructure in 90-mm lengths of the PCF could be preserved while reducing the core diameter to as little as 300nm [13].

The Sellmeier equation was used to find out the refractive index of both the core and cladding at a specific wavelength and at a specific mole fraction of germanium in the silica substrate [14], and thus the material dispersion has been taken into account. A full-vector FEM [8] has been used to characterize the PCF design.

Tailoring the dispersion to achieve flat, anomalous dispersion with small slope and zero crossing near/at the pump wavelength is an extremely important aspect in SCG. To obtain near zero ultraflattened dispersion in the middle of the visible region, we studied the tapering in and tapering out effect of the proposed geometry [15]. Thus, we optimized the proposed fiber dimension with core diameter 0.6 µm, outer cladding diameter 1.5266 µm to tailor both the ZDWs in the visible region along with its high nonlinearity parameter.

Next, the effect of outer cladding spiral air hole distribution and the defect air hole in the core are studied. Figure 4 shows the dispersion versus wavelength as a function of the diameter of the defect air hole at the center. The dispersion curve shifts down with the increase in defect air hole diameter and vice-versa. Again, the increment of the outer cladding air holes radii has an important impact on the flatness of the dispersion curve as shown in Fig. 4. The less the increment of air holes, the faster the dispersion curve bends down to lower

wavelength hampering its flatness. Thus, an optimized SSPCF shows ultraflattened dispersion (|dispersion slope|<1ps/(nm^2·km) from 580nm to 645nm) along with two zero dispersion wavelengths (ZDWs) (570nm and 630nm) in the visible region for d_c=60nm. To our knowledge, such an ultraflattened near zero dispersion of a PCF in the visible region has not been not reported before. In addition, the larger the core diameter, the broader is the range of anomalous dispersion. For a core diameter of 800nm the first and second ZDWs are at 605nm and 960nm respectively.
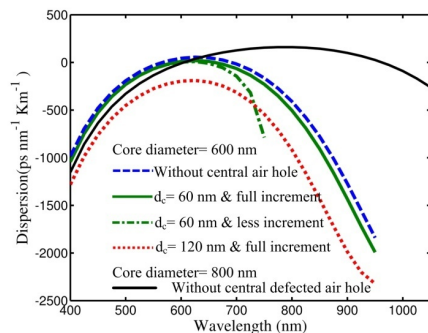

Fig. 4. Dispersion versus wavelength as a function of central air hole diameter and outer air hole increment factor.

The nonlinearity of a PCF is another important issue and in this work, we also examined the nonlinearity parameter [16], Raman gain [17], and confinement loss of the PCF we designed. The nonlinearity parameter, γ is defined as:

$$\gamma = \frac{2\pi n_2}{\lambda A_{eff}} = \frac{2\pi \iint_S n_2(x,y) I_s^2(x,y) dxdy}{\lambda \left(\iint_S I_s(x,y) dxdy \right)^2}, \qquad (1)$$

where $I_s(x,y)$ is the intensity at signal wavelength, A_{eff} is the effective area, and $n_2(x,y)$ is coordinate dependent nonlinear refractive index.

Table 1 shows the calculated values of nonlinearity parameter, effective area, peak Raman gain, and confinement loss of the PCF at different wavelengths. It can be seen that as the wavelength increases, nonlinearity and the peak Raman gain decreases due to less light confinement in the core.

Table 1
Nonlinearity parameter (γ), effective area (A_{eff}), peak Raman gain (γ_R) at (Δv) = 445cm^{-1} and confinement loss at different wavelengths (λ).

λ (nm)	γ (W^{-1}km^{-1})	A_{eff} (μm^2)	Peak γ_R (W^{-1}km^{-1})	Confinement loss (dB/Km)
575	1581	0.1838	746.105	0.000337
600	1433	0.1879	698.478	0.001611
625	1390	0.1923	653.947	0.007083

The higher the confinement in the core, the lower the A_{eff} value and hence the higher the nonlinearity and Raman gain. Moreover, it can be noticed that the fiber shows very low confinement loss (0.000337dB/km at 575nm) because of the compactness in the structure.

The proposed novel SSPCF design has tailored the two zero dispersion wavelengths around visible region (605nm and 960nm) with ultraflattened dispersion curve for a core diameter of 800nm. Moreover, we have introduced the concept of shifting the dispersion curve with the parameter of central air hole diameter and tapering. Again, the simulation for the structure shows ultrahigh nonlinearity, high Raman gain, and very low confinement loss. Due to low threshold damage in soft glass, schott SF6, and tellurite PCFs in the visible region, silica along with germanium dopant is proposed here whose threshold damage is few order magnitude higher. So, the proposed PCF may be a suitable candidate for SCG in the visible region.

References

[1] J. K. Ranka, R. S. Windeler, and A. J. Stentz, Opt. Lett. **25**, 25 (2000), http://www.opticsinfobase.org/ol/abstract.cfm?uri=ol-25-1-25

[2] J. M. Dudley, G. Genty, and S. Coen, Rev. Mod. Phys.**78**, 1135 (2006).

[3] A. Kudlinski, G. Bouwmans, M. Douay, M. Taki, and A. Mussot, J. Lightwave Technol. **27,** 1556 (2009).

[4] A. Agrawal, N. Kejalakshmy, J. Chen, B. M. A. Rahman, and K. T. V. Grattan, Opt. Lett. **33**, 2716 (2008), http://www.opticsin fobase .org /ol/abstract.cfm?uri=ol-33-22-2716

[5] A. Agrawal, N. Kejalakshmy, J. Chen, B. M. A. Rahman, and K. T. V. Grattan, IEEE Photon. Technol. Lett. **21**, 1722 (2009).

[6] C. Seaton and J. Clowes, Opt. Eng. **20**, 19 (2009), http://www.opticsinobase.org/OPN/abstract.cfm?uri=OPN-20-12-19

[7] J. Cascante Vindas, S. Torres Peiró, A. Diez M. V. Andrés, Appl. Phys. 3723 (2009).

[8] COMSOL Multiphysics, version 3.2, 2005.

[9] L. An, Z. Zheng, Z. Li, Y. Liu, T. Zhou, and J. Cheng, Asia Communications and Photonics Conference and Exhibition, ThA4, http://www.opticsinfobase.org/abstract.cfm?uri=ACP-2009-ThA4

[10] K. Saitoh, N. Florous, and M. Koshiba, Opt. Exp. **13**, 8365 (2005), http://www.opticsinfobase.org/oe/viewmedia.cfm?uri=oe-13-21-8365&seq=0

[11] K. Saitoh, M. Koshiba, T. Hasegawa, E. Sasaoka, Opt. Exp. **11**, 843 (2003). http://www.opticsinfobase.org/abstract.cfm?id=71986

[12] R. T. Bise, D. Trevor, Opt. Fiber Communication Conference **3**, 3 (2005), http://www.opticsinfobase.org /abstract.cfm ?uri=OFC-2005-OWL6

[13] S.G. Leon-Saval, T.A. Birks, W.J. Wadsworth, P.St.J. Russell, Opt. Exp. **12**, 2864 (2004) http://www.opticsinfobase.org/oe/abstract.cfm?id=80305

[14] C. K. F. Ho, K. Pita, N.Q. Ngo, and C.H. Kam, Opt. Exp. **13**, 1049 (2005), http://www.opticsinfobase.org/oe/abstract.cfm?URI=OPEX-13-3-1049

[15] S. Roy, K. Mondal, and P. Roy Chaudhuri, Appl. Opt. **48**, G106, (2009), http://www.opticsinfobase.org/abstract.cfm?uri=ao-48-31-G106

[16] T. Sun, G. Kai, Z. Wang, S. Yuan, and X. Dong, Chinese Opt. Lett. **6**, 93 (2008).

[17] J. Bromage, K. Rottwitt, and M. E. Lines, IEEE Photon. Technol. Lett. **14**, 24 (2002).